Fuel Pellet Thermal Analysis

K M Zaheen Nasir

February 2024

1 Introduction

Recent undertakings in the nuclear power engineering community for increasing the life of LWR reactors and their constituents necessitate critical analysis of the prevalent fuel types in terms of their longevity, economy, performance at high burn-up, and temperature. Consequently, thermal analysis of LWR fuel pellets is an important stepping stone for analyzing the critical thermo-mechanical performance of the fuel and its interaction with the surroundings. This is primarily because microstructure and material properties inside the fuel change as a function of temperature with time. Therefore, in this project (part 1), thermal analysis of a UO_2 fuel pellet is performed in an axisymmetric manner in RZ coordinate. The given pellet geometry is shown in Figure 1. Both steady and transient thermal analyses have been performed for constant and temperature-dependent thermal conductivity of fuel and gap. Cladding thermal conductivity was taken as constant in all cases. Table 1 provides the material-specific thermal parameters considered for these analyses.

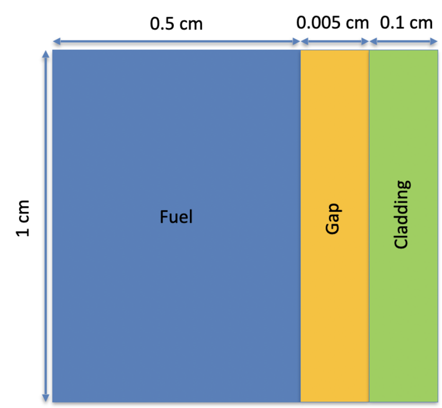

Figure 1: Pellet Geometry in RZ Coordinate (Axisymmetic 2D).

Quantity	Symbol	Value/Function
Outer Cladding Temperature	T_{CO}	550 K
Fuel Thermal Conductivity Constant	K_F	0.03 $W/(cm*K)$
Fuel Thermal Conductivity Temp Dependent	K_{FT}	$K_{FT} = 1/(A+BT)$, $A = 3.8 + 200 * FIMA$, $B = 0.0217$
Gap Thermal Conductivity Constant	K_g	0.002556 $W/(cm*K)$
Gap Thermal Conductivity Temp Dependent	K_{gT}	$(16*10^{-6})*T^{0.79}$ $W/(cm*K)$
Cladding Thermal Conductivity	K_C	0.17 $W/(cm*K)$
LHR Steady	LHR	350 W/cm^2
LHR Transient	LHR	$250*exp(-((t-20)^2)/10)+150$ W/cm^2

Table 1: Material Specific Thermal Parameters for Fuel Pellet

2 Meshing

The given geometry was meshed using the **GeneratedMeshGenerator** moose object. For the steady state analyses, we adopted a 1000 x 1000 elements mesh along R and Z directions respectively. Although a good FEM analysis requires a balanced aspect ratio for each element's dimensions, the same number of elements in each dimension were used for this simple geometry without increasing the element number in Z direction. Moose object **SubdomainBoundingBoxGenerator** were used to further subdivide the domain into three blocks representing fuel, gap, and cladding. Figure 2 shows the subdivisions of the problem domain. An element number of 1000 is chosen in the R direction so that the element size (0.000605 cm) remains smaller than the gap width and the mesh object can easily recognize the gap block. However, any element size smaller than the gap size would've also worked. Similarly, we maintained the same number of elements for transient analyses as well.

3 Kernels, Variables and Boundary Conditions

Thermal analyses of the fuel pellet were done using the basic heat conduction equation as the governing equation over the problem domain. The strong and weak forms of the governing equations are presented below.

Strong Form:

$$\rho C_p \frac{\partial T}{\partial t} = \nabla.(k \nabla T) + Q \tag{1}$$

where ρ is the density, C_p is the specific heat, T represents the temperature

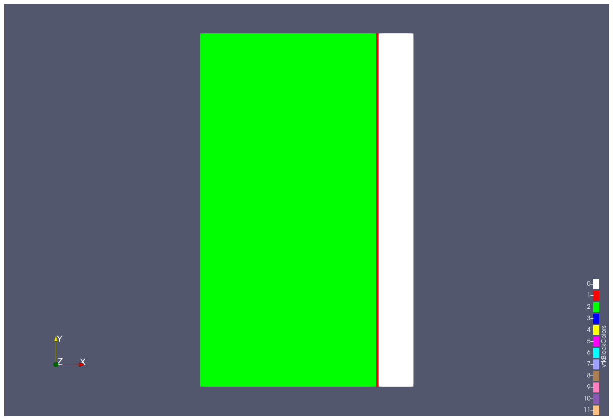

Figure 2: Mesh blocks representing fuel(Green), gap(red), cladding(white).

profile of the fuel pellet and Q is the heat source.

Weak Form:

$$(\phi_i, \rho C_p \frac{\partial T}{\partial t}) + (\nabla \phi_i, k \nabla T) - \langle \phi_i, k \nabla T.\mathbf{n} \rangle + (\phi_i, Q) = 0 \qquad (2)$$

where ϕ_i is the FEM weighting or trial function and **n** is the outward vector normal to the boundary. We obtain equation 2 (weak form) from the strong form of the heat conduction equation as per Galerkin formulation where the trial functions are the same as the FEM shape functions. Observing the weak form we automatically understand that the MOOSE implementation requires three kernels for transient analysis for the terms shown within the parenthesis in Equation 2. Number of required kernels are reduced to two for steady-state analysis. We chose **HeatConduction**, **HeatSource**, and **SpecificHeatConductionTimeDerivative** as the kernels of the said analysis. Standard formulation were used to convert **LHR** to heat source **Q** as an input to the **HeatSource** kernel. The weak form also reveals the necessity of Neuman BC represented by the term within the angular brackets. On the other hand, Dirichlet BCs are directly implemented within the FEM shape function. Therefore, we apply Neuman BC of $\nabla T = 0$ on the left boundary representing the centerline of the fuel and T = 550 K on the right boundary as cladding outer temperature. The scalar variable temperature is taken as the primary variable representing our required solution field.

4 Choice of Materials

Our analyses were strictly kept within the LWR scenario. As a result, we chose UO_2 as our fuel material with Zircaloy-4 cladding. Helium is taken as the gas occupying the gap between fuel and cladding material. Their material properties used in the simulations except for thermal conductivity (already given in table 1) are listed in table 2.

Properties	UO_2	He	Zircaloy-4	Units
Density	10.98	$0.178 * 10^{-3}$	6.5	g/cm^3
Specific Heat	0.33	5.188	0.35	$J/g-K$

Table 2: Material properties used for the Analyses.

5 Results

Considering helium in the gap we obtained the following analytical solution for the steady state.

$$\frac{\mathbf{LHR}}{2\pi R_F} = \frac{350}{2\pi 0.5} = 111.408$$

Cladding inner temperature:

$$\therefore T_{CI} = T_{CO} + \frac{\mathbf{LHR}.t_c}{2\pi R_F.K_C} = 550 + 111.408\frac{0.1}{0.17} = 615.534\ K$$

Assuming $T_{CI} = T$ we have,

$$K_g = 16 * 10^{-6} * T^{0.79} = 0.002556\ W/(cm.K)$$

$$h_{gap} = \frac{K_g}{t_g} = \frac{0.002556}{0.005} = 0.5112\ W/(cm^2.K)$$

Fuel surface temperature:

$$\therefore T_S = T_{CI} + \frac{\mathbf{LHR}}{2\pi R_F.h_{gap}} = 615.534 + \frac{111.408}{0.5112} = 833.46\ K$$

Fuel centerline temperature:

$$\therefore T_o = T_S + \frac{\mathbf{LHR}}{4\pi K_F} = 833.46 + \frac{350}{4\pi 0.03} = 1761.86\ K$$

The results of the analyses along with the comparison of steady state solution with our analytical one are portrayed in table 3.

The contour plots and the spatial profiles of temperature along the radial direction of the fuel pellet including gap and cladding for both constant and temperature-dependent thermal conductivity of the steady state analyses are presented in figure 3 and 4 respectively.

Similar plots including the temporal profile of fuel centerline temperature up to 100 sec for both constant and temperature-dependent thermal conductivity are shown in figure 5 and 6 respectively.

Properties	**Steady-Const. K**	**% Error**	**Steady-Temp. dep. K**	**Transient-Const. K**	**Transient-Temp. dep. K**
Fuel centerline temp.(K)	1772.35	0.595	1642.95	1073.88	925.843
Fuel surface temp.(K)	844.943	1.378	818.943	676.407	675.377
Cladding inner temp.(K)	609.023	1.058	609.023	575.296	575.296
Cladding outer temp.(K)	550	0	550	550	550
Approach to steady state (sec)	-	-	-	50	45
Steady-state reached (sec)	-	-	-	85	72

Table 3: Analyses results and comparison with analytical solution.

6 Discussion

Comparison with the analytical solution for the steady state reveals negligible errors and points towards successful modeling of the fuel pellet temperature profile. According to our empirical dependence of thermal conductivity upon temperature as used in the simulation, fuel thermal conductivity decreases with increasing temperature while gap conductivity increases. However, as observed from our analysis, this had an overall effect of decreasing the fuel centerline temperature resulting in a lower thermal gradient across the fuel pellet compared to constant thermal conductivity. During the transient analyses, it was observed that the nonlinear solve fails to converge when the steady state is approached. This is because the nonlinear Newton-Raphson fails to find a suitable value for the scalar variable temperature that minimizes the residual beyond the set tolerance. The fact that the temperature doesn't deviate much due to the approaching steady state contributes to the inability of Newton-Raphson to minimize the residual beyond a certain value. This problem required a workaround by changing the nonlinear tolerances in the executioner block. We set **nl_rel_tol = 1e-10** and **nl_abs_tol = 1e-10** to obtain our transient solution. Transient analysis showed a peaking of the fuel centerline temperature at 23 sec reaching 1414.15 K and 1285.82 K for constant and temperature depen-

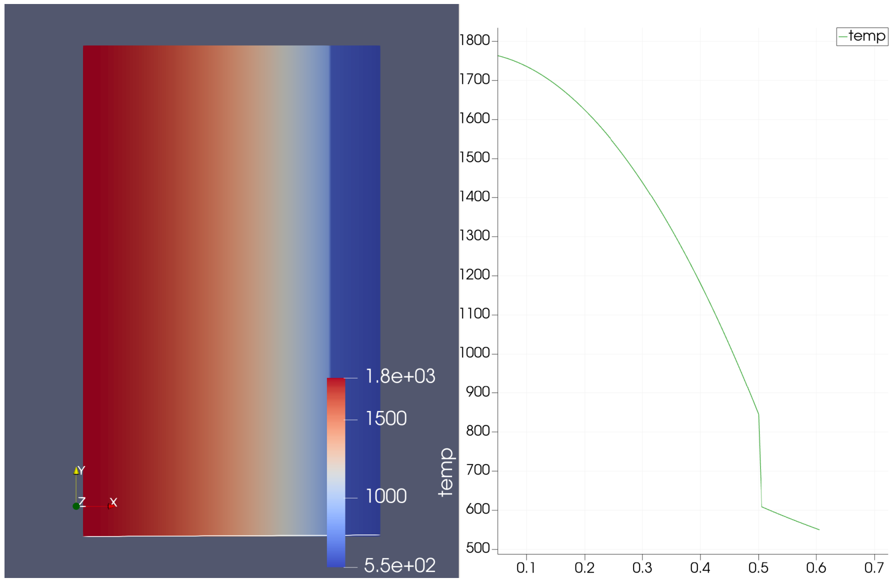

Figure 3: Contour and spatial temperature profile for constant thermal conductivity in steady state.

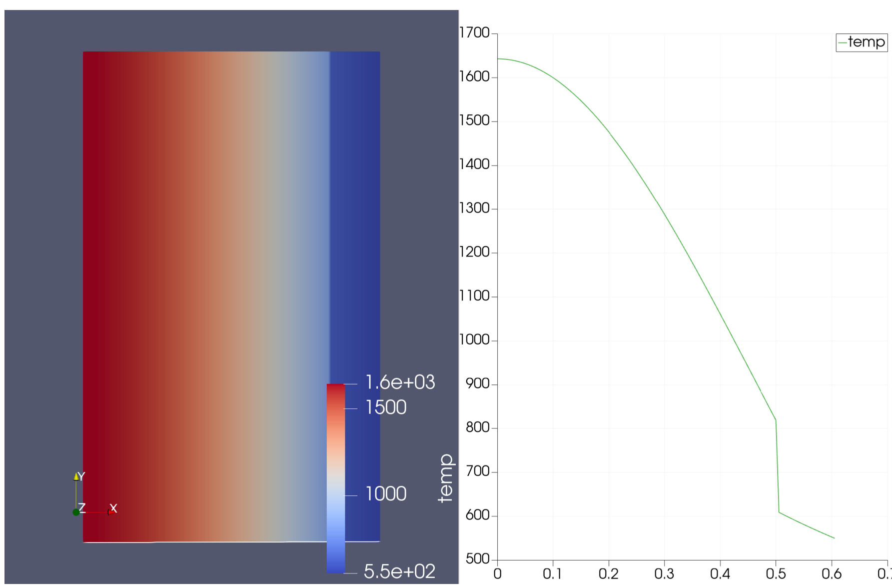

Figure 4: Contour and spatial temperature profile for temperature-dependent thermal conductivity in steady state.

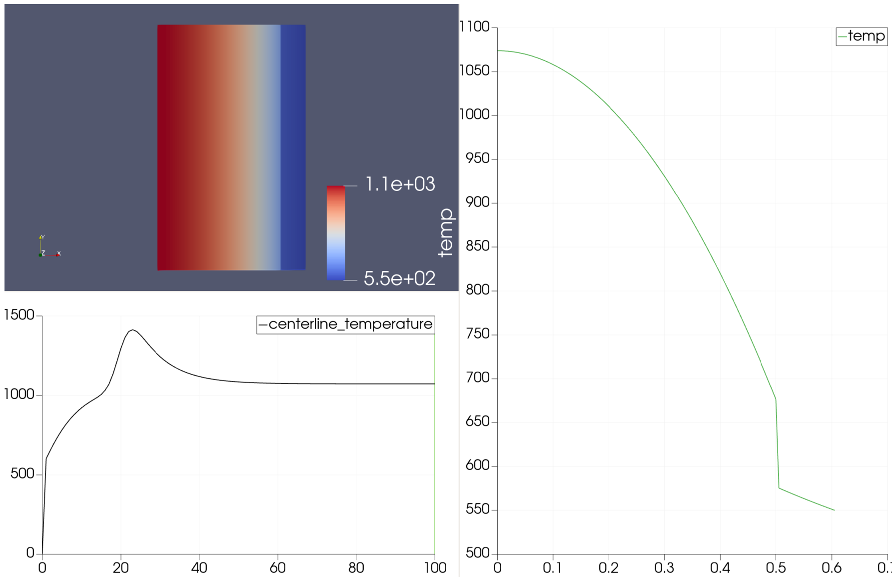

Figure 5: Contour, spatial temperature, and temporal fuel centerline temperature profile for constant thermal conductivity.

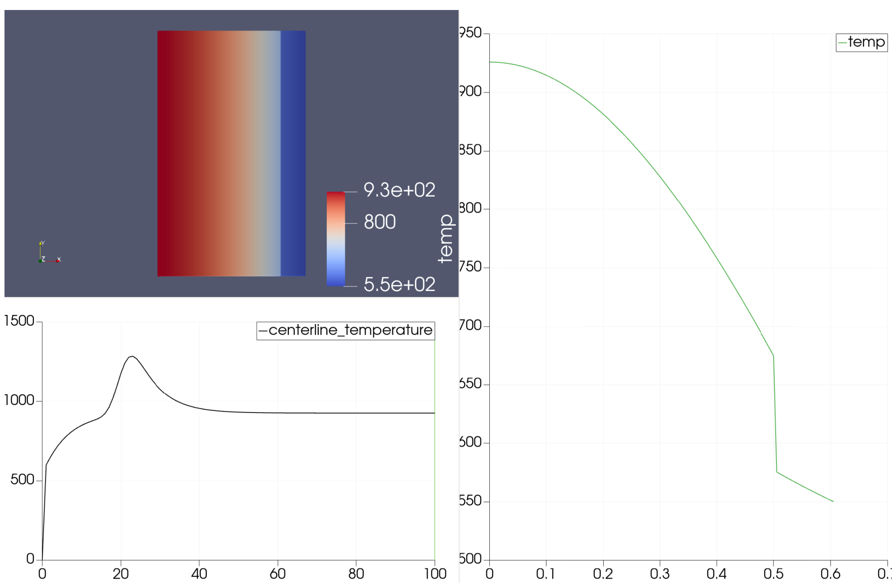

Figure 6: Contour, spatial temperature, and temporal fuel centerline temperature profile for temperature-dependent thermal conductivity.

dent thermal conductivity before reaching respective steady state. We used a post-processor object of **SideExtremeValue** to track the fuel centerline temperature.

7 Conclusion

Accomplishing this project has equipped us with hands-on knowledge of modeling fuel pellet temperature using MOOSE. Although MOOSE is a powerful modular and pluggable framework for performing a wide range of analyses, a thorough understanding of physics behind the problem and numerical schemes such as FEM, implicit time integration using Newton-Raphson or Preconditioned Jacobian Free Newton Krylov (PJFNK) etc in solving the problem is essential. Obtaining a transient solution by tweaking the tolerances that don't deviate from the expected behavior according to the physics of the problem domain is a testament to this requirement. Eventually, it will allow us to perform any kind of large-scale analysis using any type of modeling tool similar to MOOSE.